ELSEVIER

Polymer 42 (2001) 651–665

polymer

www.elsevier.nl/locate/polymer

The effects of branching and fibre drawing on the crystal structure of polyethylene

A.M.E. Baker[1], A.H. Windle*

Department of Materials Science and Metallurgy, Pembroke Street, Cambridge CB2 3QZ, UK

Received 4 February 1999; received in revised form 27 March 2000; accepted 12 April 2000

Abstract

The structural characterisation of a broad series of commercial branched polyethylenes in both unoriented and uniaxially drawn fibre sample forms is described, using differential scanning calorimetry and X-ray diffraction. The influences on the crystal structure of polyethylene of branch content, type and distribution, and also uniaxial fibre drawing, have been determined. As well as providing a comprehensive analysis of the effect of branching, this paper also forms the basis for two further papers on this series of polyethylenes. These associated papers examine more intricate aspects of the structure of polyethylene: a partially ordered component and the accommodation of the short chain branches within the crystalline structure.

To enable direct comparison between all structures, the unoriented samples were prepared under a common set of conditions and the fibre samples were drawn from these unoriented samples. Fibre drawing reduced the three crystal unit cell parameters for most grades and for all grades an increase in crystalline density was seen. The unit cell parameters of the fibre samples spanned broader ranges than the unoriented samples. Regarding branching parameters, for both unoriented and fibre samples, the *a* and *b* unit cell parameters increased with branch content, although with considerable scatter. Some of this scatter in the fibre samples was found to be explained by differences in the branch distribution of the grades: for similar branch contents, randomly placed branches generally produced higher unit cell expansions than heterogeneously placed branches. For ethyl and longer branch types, it is generally believed that for a given concentration, there is little if any effect of branch type on the extent of expansion caused. In this study, however, different degrees of expansion were apparent in the longest unit cell parameter (the *a* parameter) of the fibre samples, where the range of values seen across samples was largest. In these samples, for similar branch contents of ethyl, butyl, isobutyl and hexyl branches, hexyl branches caused the most expansion and ethyl branches the least expansion.

Keywords: Polyethylene branch content, type and distribution; Crystalline structure; Uniaxial fibre drawing

1. Introduction

The diversity in structure and properties of polyethylene is achieved by copolymerisation of the ethylene monomer with a low concentration of one or several α-olefin comonomers, producing branches off from the main polyethylene backbone. Further variations are possible by changing the polymerisation process conditions and the choice of catalyst. These factors can affect, for example, the average molecular weight and its distribution [1] and the branch content and placement along the polyethylene chains [2], whether uniform, random, or clustered (heterogeneous). New catalyst systems are still emerging, the most important in recent years being the metallocenes in 1991.

The structural variations which exist between different grades together with the vast number of grades make polyethylene an ideal and unique system for studying the effect that small changes in structure at the molecular level have on the polymer's larger-scale structure, and thereby its physical properties. To date, however, structural studies concerning branching in polyethylene have generally been confined to investigating the influences of branch content and branch type on the structure [3–18] whilst the possible influence of branch distribution has largely been ignored and not treated objectively. In this study we present an objective analysis of the effect of branch distribution on the crystal structure of polyethylene.

The standard method of classifying polyethylenes is via the number and type of short chains branches per 1000

* Corresponding author. Tel.: +44-1223-334321; fax: +44-1223-334300.

E-mail address: ahwl@cus.cam.ac.uk (A.H. Windle).

[1] Present address: MRC Laboratory of Molecular Biology, Hills Road, Cambridge CB2 2QH, UK.

0032-3861/01/$ - see front matter
PII: S0032-3861(00)00363-3

carbon atoms (SCB/1000C) along the polyethylene backbone, including the carbon atoms of the branches themselves. This description neglects how the branches are arranged along and between the chains, namely intramolecular and intermolecular heterogeneity. The positioning of these α-olefin branches is difficult to control although it is known that the catalyst and process conditions used are important factors. Heterogeneity in branch distribution affects the crystallisation behaviour and material properties of the polyethylene [19,20]. Amongst commercial grades, LDPE is an example of nearly random branch placement because of the free radical polymerisation process used. LLDPE, which forms the basis of this study, contains both intermolecular and intramolecular heterogeneity.

In previous studies of the effects of branching on polyethylene structure, the influence of branch distribution has been ignored, primarily because of the lack of a technique known to assess heterogeneity satisfactorily. Analytical temperature rising elution fractionation (TREF) has since evolved and is capable of parametrising branch heterogeneity [21]. This technique is based on the principle that for a polymer sample in an ideal solvent, the chains will crystallise over a range of temperatures according to differences in molecular structure [22–24]. In the case of polyethylene, the crystallisation temperature of each chain for a given molecular weight will be determined by the longest sequence of methylene units between branch points in that chain, *N*. In TREF, the distribution of branch points within a sample is referred to as the methylene sequence length distribution. It is defined as the ratio of number ($\bar{N}_n$) and weight ($\bar{N}_w$) averages of *N*, namely $\bar{N}_w/\bar{N}_n$. This is analogous to the molecular weight distribution parameter $\bar{M}_w/\bar{M}_n$.

In this paper we investigate the effects of branch content and branch type on the crystal structure of branched polyethylenes using an unusually large set of samples, in both unoriented and uniaxially drawn fibre sample forms. In addition the effect of branch distribution is examined for the first time. Samples were characterised by differential scanning calorimetry (DSC) and their crystal structure parameters determined by X-ray diffraction. The crystal structure parameters were analysed with respect to molecular structure parameters determined from ^{13}C NMR and analytical TREF. This paper is the first of three investigating the structure of these 15 branched polyethylenes. The second paper [25] presents evidence from the X-ray diffraction patterns for a partially ordered component. The third paper [26] investigates the location of the short chain branches (exclusion versus inclusion) by combining the X-ray diffraction data with molecular modelling studies. Together the sequence of three papers presents a comprehensive and original examination of the structure of branched polyethylene, linking new methods in X-ray diffraction pattern recording and analysis to molecular modelling.

2. Methods

2.1. Materials

Fifteen grades of commercial polyethylene were examined and details are given in Table 1: three grades of unbranched HDPE (high density polyethylene) referred to as homopolymers, two grades of lightly methyl-branched HDPE, two grades of LDPE (low density polyethylene), seven grades of LLDPE (linear low density polyethylene) and one grade of VLDPE (very low density polyethylene). Molecular characterisation data for the 15 grades are listed in Table 1 as well as sample identifiers which will be used hereafter. For all grades except LDPE, the branch contents were known to an accuracy of at least ±0.5 SCB/1000C from ^{13}C NMR and ranged from fewer than 0.5 SCB/1000C for the HDPE homopolymers (assumed in all data analyses here to be 0 SCB/1000C) to 30.5 SCB/1000C for the VLDPE. The branch types ranged from methyl to hexyl. For LDPE, the complex branching present, including long chain branching, hinders analysis by ^{13}C NMR [27]. For the two LDPE grades used here the branch content was estimated from previous studies on similar samples [28–30] to be 12 SCB/1000C (various olefin branches although mainly ethyl and butyl).

Fourteen of the grades were supplied as pellets and were hot-pressed into unoriented mats. One homopolymer HDPE grade, *hom_c*, was supplied only in fibre form and another of the homopolymer grades, *hom_a*, would not draw successfully because of its low molecular weight. Thus 14 grades were examined in unoriented form and 14 grades in fibre form, 13 of the grades being common to both sample forms. The sample forms examined for each grade are shown in Table 1 by the symbol type used for that sample in all graphs throughout the paper: the absence of a symbol indicates that the sample form for that grade was not available.

2.2. Sample preparation

The unit cell parameters of polyethylenes depend on crystallisation conditions, annealing treatment and deformation, as well as branching parameters [17,31–33]. In order to focus on the influences of branching and fibre drawing, all unoriented samples were made under a common set of crystallisation conditions, without subsequent annealing treatment; the fibres were drawn from these unoriented samples. An exception was *hom_c* which was supplied ready-drawn into fibres. The overall consistency in sample preparation allowed confidence that any variations observed between the structures would relate primarily to chemical differences between the materials, such as the branching, rather than to differences in thermal treatment.

The unoriented samples were produced by hot-pressing at 180°C, 2500 psi, with a cooling rate of 15°C min^{-1} to a sample thickness of either 1.05 ± 0.03 or 0.80 ± 0.03 mm. Uniaxially oriented fibre samples

Table 1
Characterisation data for the 15 grades of branched polyethylene

Sample ID	Material	Branch type [NMR]	Branch conc. (SCB/1000C) [NMR]	Branch distribution [TREF]		Density (kg m^{-3})	Mol wt $M_w/10^3$ [GPC]	Mol wt distribution (M_w/M_n) [GPC]	Unoriented sample graph symbol	Fibre sample graph symbol	Fibre drawing	
				N_w/N_n	Random (r) or hetero geneous (h)						Temp. /°C	Draw ratio
hom_a[a]	HDPE	Olefin	<0.5	–	–	962	66	4.4	◇		–	
hom_b[a]	HDPE	Olefin	<0.1	–	–	960	130	7.6	◇	◆	90	10.0
hom_c[a]	HDPE	Olefin	<0.5	–	–	960	100	6.2		◆	125	40
meth_4	HDPE	Methyl	4	–	r[b]	–	–	–	▽	▼	90	11.7
meth_5	HDPE	Methyl	5	–	r[b]	–	–	–	▽	▼	90	10.3
eth_16	LLDPE	Ethyl	15.5	1.39	r	920	128	4.0	○	●	90	9.9
eth_18	LLDPE	Ethyl	18	1.73	h	919	124	4.8	○	●	90	10.2
eth_31	VLDPE	Ethyl	30.5	1.62	h	905	134	3.8	○	●	75	9.7
isob_14	LLDPE	Isobutyl	13.8	1.66	h	918	96	3.2	□	■	90	9.8
but_15	LLDPE	Butyl	15	1.85	h	918	119	3.7	□	■	90	10.0
hex_12	LLDPE	Hexyl	12.4	1.92	h	922	–	–	△	▲	75	8.3
hex_14a	LLDPE	Hexyl	14	1.44	r	920	128	4.8	△	▲	90	9.4
hex_14b	LLDPE	Hexyl	14	1.36	r	920	111	4.0	△	▲	80	9.2
ldpe_a	LDPE	Olefin	12[c]	–	r[b]	920	92	5.4	×	+	90	6.2
ldpe_b	LDPE	Olefin	12[c]	–	r[b]	920	96	5.6	×	+	90	6.4

[a] 'hom' is an abbreviation for 'homopolymer', or unbranched HDPE. In practice polyethylene homopolymers do contain very low concentrations of various olefin branches, here <0.5 SCB/1000C. For simplicity, all data analyses in the paper assume a branch content for these three homopolymer HDPE grades of 0 SCB/1000C.

[b] The methyl-branched HDPE and LDPE grades were not suitable for TREF evaluation, so $\bar{N}_w/\bar{N}_n$ values are not available. Nevertheless, the branch distribution of HDPE is approximately random whilst that of LDPE is almost ideally random. The samples used in all the $\bar{N}_w/\bar{N}_n$ branch distribution analyses are the seven LLDPE grades; the HDPE and LDPE grades feature only qualitatively in Fig. 8.

[c] Estimated from Refs. [28–30].

were drawn from dumb-bells cut from the unoriented samples. The nominal draw ratio was 10, at 50 mm min^{-1} in an air oven, at a temperature between 75–90°C. The actual draw temperature for each grade was set to approximately 40°C below the melting point (determined by DSC, see Fig. 3) to ease some of the structural distortion. An exception was made for the LDPE grades because their low melting temperature of around 110°C and consequently low draw temperature compounded with the presence of long-chain branching meant that breakage of the fibres occurred before a draw ratio of 10 could be reached. Therefore, for the LDPE samples, a temperature of 90°C was used to obtain a draw ratio as near to 10 as possible. The effects of draw ratio and temperature on the structure and morphology of polyethylene have been well-researched although they remain controversial [34–39]. A draw ratio of 10 was chosen here to orientate the crystallites sufficiently for fibre diffraction whilst minimising disruption to the structure [40]. Table 1 shows the actual draw temperatures used and the draw ratios achieved which were in the range 9.2–11.7 for the HDPE, LLDPE and VLDPE grades (except *hom_c* supplied ready-drawn) and 6.2–6.4 for the LDPE grades. The fibre thicknesses obtained were in the range 0.32–0.38 mm.

2.3. Analytical TREF

An estimate of the heterogeneity in branch distribution of the grades was obtained by the TREF method of Bonner et al. [21] although TREF has some limitations. TREF is valid only for relatively highly branched polyethylene grades (>10 SCB/1000C) such as LLDPE and VLDPE where *N*, the longest sequence of methylene units between branch points in a chain, is less than or equal to the chain fold length. Also, neighbouring or very closely spaced branches which produce nil or very small methylene sequence lengths are not accessible. TREF is better suited to assessing intermolecular heterogeneity since this rather than intramolecular heterogeneity is the more influential factor during the TREF process. Where intramolecular heterogeneity is present as well as intermolecular heterogeneity, this leads to some uncertainty in interpretation of the $\bar{N}_w/\bar{N}_n$ parameter value obtained. In spite of these limitations, TREF nevertheless allows a quantitative estimate of the relative degree of heterogeneity in branch placement between samples and is the best method currently available for this purpose.

The TREF data collection and analysis were performed by BP Chemicals, Grangemouth. A 30 cm TREF column was packed with inert support material to provide maximum surface area for crystallisation. Samples were dissolved in 1,2,4-trichlorobenzene at 140°C to a concentration of 0.002 g cm^{-3}, introduced into the TREF column and allowed to cool at 1.0°C h^{-1}. 1,2,4-trichlorobenzene eluant was then washed through the column whilst the temperature was raised at 20°C h^{-1} from 22 to 130°C and the eluate analysed simultaneously by a Miran infra-red detector tuned to 3.48 μm, the C–H bond stretch frequency. The branching distribution parameters were calculated using the method of Bonner et al. [21].

Table 1 lists $\bar{N}_w/\bar{N}_n$ values for some of the samples. A $\bar{N}_w/\bar{N}_n$ value of 1.0 indicates uniform branch placement and empirically, $\bar{N}_w/\bar{N}_n$ values around 1.3 have been found for grades known to be essentially randomly branched; higher values indicate increasing levels of heterogeneity. Accordingly, the grades are classified in Table 1 as random 'r' or heterogeneous 'h' although this sample labelling is not used in any of the data analyses. $\bar{N}_w/\bar{N}_n$ values were not available for the two LDPE grades, nor for the lightly methyl-branched HDPE grades. Nevertheless, the branch distribution of methyl-branched HDPE is believed to be approximately random whilst that of LDPE is almost ideally random and so 'random' labels are assigned in Table 1. All the $\bar{N}_w/\bar{N}_n$ branch distribution analyses, however, use only the seven LLDPE grades; the HDPE and LDPE grades feature only qualitatively in Fig. 8.

2.4. DSC

Samples with mass in the range 5.00 ± 0.50 mg were cut from the unoriented and oriented samples. A Perkin–Elmer DSC 7 calorimeter was used, with heating and cooling rates of 10°C min^{-1} over the temperature range −40–150°C. The ramp rate of 10°C min^{-1} was chosen to minimise structural reorganisation during heating whilst ensuring that reliable melting temperatures could be obtained [41]. The sub-ambient start temperature was used because of the broad crystallisation range in branched polyethylenes [42]. The degree of crystallinity in each sample was calculated from the heat of melting of the first heating run, to enable comparison with the value calculated from X-ray diffraction. The melting endotherms were determined by fitting a sigmoidal baseline to each DSC trace; the heat of fusion for all the polyethylene grades was assumed to be 292 J g^{-1} [43]. For calculating the melting temperature, T_m, from a DSC trace, there are several methods with varying degrees of sophistication [44]. Here a consistent, simple method of estimation was required and was taken to be the peak position of the highest temperature endotherm, since this endotherm represents melting of the relatively highly crystalline material within the sample. The melting temperature was then used to estimate the lamellar thickness of this component via the Thomson–Gibbs equation [45] (with values of the equilibrium melting temperature of an infinite crystal, T_m^∞ as 146.0°C; the surface free energy of a crystallite (upper and lower surfaces), σ_e, as 60.9×10^{-3} J m^{-2}, and the heat of fusion per unit volume of crystal, ΔH_c, as 2.88×10^8 J m^{-3}). Corrections such as for heating rate and sample size were not considered necessary nor justified because assumptions implicit in the Thomson–Gibbs equation (for example of thermodynamic

equilibrium) were known not to be met by the DSC conditions.

2.5. X-ray diffraction from unoriented (powder) samples

X-ray diffraction patterns from the unoriented samples were recorded from 10–60°2θ in reflection and transmission modes at 40 kV, 40 mA using a Siemens D500 $\theta/2\theta$ vertical diffractometer with 2.2 kW sealed tube source (copper target) and secondary Soller slits. Transmission scans have poorer resolution and poorer counting statistics for a given counting time and were used only for comparison of peak intensity ratios with the reflection mode data as a test for preferred orientation in a plane normal to the plane of the samples. This comparison revealed that most of the samples had very slight preferred orientation with the *b*-axis of the orthorhombic crystal structure of polyethylene preferentially oriented normal to plane of the samples [46–48]. The preferred orientation was more noticeable in the thinner samples (0.8 mm). Flat-plate X-ray transmission photographs demonstrated that all samples were unoriented within the plane of the samples. All analyses described here were applied to the reflection mode data. For these scans, parafocusing geometry was used with a secondary beam monochromator, a divergence slit of 0.3°, two antiscatter slits of 0.3° and a receiving slit of 0.15°. Primary Soller slits were additionally used in some reflection scan data sets, to maximise resolution although no significant improvement was noted. A step size of either 0.10°2θ or 0.05°2θ was used. Silicon powder was used in early trials to confirm and test the reproducibility of alignment of the surfaces of the samples with the goniometer axis.

Degree of crystallinity estimates were made by unconstrained fitting (i.e. without crystal structure information) of the data below 28°2θ since this region contains most of the coherent scattering from polyethylene. The intensity data were fitted to the two crystalline reflections (110) and (200) near 22°2θ, the amorphous halo centred around 19°2θ and a linear background. The crystallinity was calculated as the ratio of the sum of the areas of the two crystalline peaks to that of the sum of the two crystalline peaks with the amorphous halo. More refined methods have been devised [12,49–53] although the different estimates are not consistent one with another. Since crystallinity values were of only peripheral interest in this study, we preferred to use the method outlined above which had the merit of simplicity.

A correction to the X-ray diffraction patterns was made for sample transparency, according to the method of Langford and Wilson [54] as well as for Lorentz and polarisation effects. Correction for sample transparency is rarely made in X-ray diffraction studies; the correction and its importance relative to Lorentz and polarisation factors are described in Appendix A. The sample transparency correction was applied to the raw reflection mode diffraction data on a point-by-point basis, as shown in Appendix A, Fig. A1. The Lorentz and polarisation factors were applied, also on a point-by-point basis, via the analysis software used: Philips PC-Rietveld Plus v1.1B [55]. The polarisation factor used included a contribution from the secondary graphite monochromator used in data collection [66] (see Fig. A1).

The X-ray diffraction patterns were fitted using the Rietveld method, a whole pattern fitting structural refinement process [56,57]. It was used as a consistent method of fitting the diffraction patterns with the aim of refining cell parameters and peak intensities. The two dominant reflections, (110) and (200), were excluded from the fitting procedure because they were believed to be affected by the presence of a partially ordered component, as described in the following paper [25]. Fitting was therefore performed within the range 28–60°2θ, covering 16 reflections. CuKα_1 and CuKα_2 wavelength contributions were included in the fitting assuming an intensity ratio $\alpha_2/\alpha_1 = 0.5$. The diffraction peaks were fitted using the pseudo-Voigt profile, a flexible profile commonly used for fitting the relatively poor quality diffraction patterns from polymers [58]. Peak widths were fitted using the Cagliotti equation [59] which, although intended for neutron diffraction data, is still in widespread use in X-ray diffraction profile analysis [57] because of the lack of a more accurate yet simple enough expression. It was not found necessary to refine the atomic coordinates of polyethylene [60]. The amorphous scattering was fitted to two broad peaks [39], one from inter-chain interactions, at 19.6°2θ and the other from intra-chain interactions, at 42°2θ [61]. A background of the form $y_{ib} = c + k\theta_i^2$ was used. The March model [62] was used to account for the low levels of preferred orientation detected in some of the samples as mentioned earlier.

2.6. X-ray diffraction from uniaxially oriented (fibre) samples

The fibre X-ray diffraction patterns were recorded in symmetric transmission mode using a novel fibre diffractometer based on a scanning CCD camera, recently designed and built in our laboratory [63,64]. CuKα radiation at 40 kV, 55 mA was used, with a germanium primary focusing monochromator. The principal attributes of the system were the ability to access all the diffraction data available from a fibre sample and to map the data into cylindrically averaged reciprocal space to produce an undistorted image. Each complete, composite fibre pattern out to 80°2θ was mapped from approximately 200 separate images at different reciprocal space positions. Before mapping, each image was corrected for non-uniformity of the detector response by dividing it by the image recorded under uniform illumination of the camera surface by an americium beta source with copper target. Silicon powder was used as an internal standard.

In contrast to the unoriented diffraction data, Lorentz, polarisation and transparency corrections were not applied for the following reasons. For the Lorentz factor, uncertainty

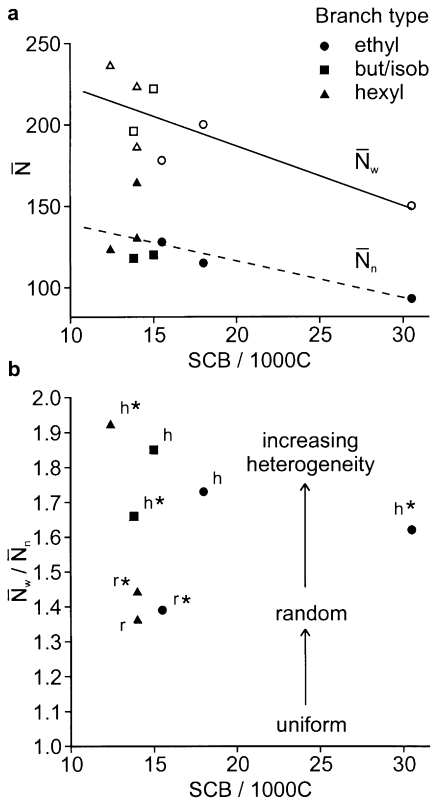

Fig. 1. Analytical TREF data showing the variation in distribution of branches in the seven LLDPE grades (branch contents around 15 SCB/1000C) and one VLDPE grade (31 SCB/1000C). (a) The number and weight average methylene sequences, $\bar{N}_n$ (solid symbols) and $\bar{N}_w$ (open symbols), respectively. (b) The branch distribution parameter $\bar{N}_w/\bar{N}_n$. The possible values of $\bar{N}_w/\bar{N}_n$ range from 1.0 (uniform branch placement) up through 1.1–1.3 (random branch placement) to higher values which indicate increasing levels of heterogeneity in branch placement [69]. In (b) the sample data-points have been identified by their $\bar{N}_w/\bar{N}_n$ value as either approximately random (r) or approximately heterogeneous (h) in branch distribution. The data-points in (b) additionally identified by * indicate grades where, from DSC, the main melting endotherm of the unoriented sample was divided into three peaks (refer to Fig. 2). The linear regression fits in (a) are shown by a solid line if the slope was significantly different from zero ($P < 0.05$, *t*-test), dotted otherwise. As expected, $\bar{N}_n$ and $\bar{N}_w$ show a decrease with increasing branch content. No relationship is seen between the distribution of branches and the number of peaks in the melting endotherm.

exists in its form for fibre diffraction: it is usually assumed to be the same as for a rotating single crystal under the same conditions. However, separate expressions for the factor depending on the type of reflection, whether equatorial (*hk*0), meridional (00l) or general (*hkl*), have been argued to be more satisfactory [65]. Regarding the transparency error, the fibres were considerably thinner than the unoriented samples, which meant that the necessary correction factor for the symmetric transmission mode used [66] at 60°2θ normalised with respect to that at 20°2θ (the range of 2θ values where polyethylene reflections were analysed) was nearly 1 (0.92). This ratio contrasts with the more influential ratio of 0.57 (see Fig. A1b) for the transparency correction calculated for the unoriented sample diffraction data.

The fibre diffraction patterns were fitted using the CCP13 fibre diffraction software (Daresbury Laboratory); this refined the cell parameters and reflection intensities but did not include full structural refinement. As for the unoriented samples, the two dominant reflections (110) and (200) were omitted from the fitting procedure because they were believed to be affected by the presence of a partially ordered component, as described in the following paper [25]. Fitting was performed on the five equatorial reflections in the range 28–46°2θ and the first seven reflections along the first layer line (out to 60°2θ) i.e. 12 reflections in total. Unlike the unoriented sample data, only a single peak of weighted average wavelength was fitted to each reflection, representing both CuKα_1 and CuKα_2 contributions. The broadness of the reflections from the polyethylene fibres because of crystal size/strain effects meant that the presence of two contributions to each reflection could not be detected and that fitting of two wavelength contributions was not meaningful. The amorphous scattering contribution was fitted as part of the background scattering. Separate refinements using both Gaussian, Lorentzian and mod. 2 Lorentzian profiles were performed and compared. A dependence was noted between the *R*-factors for the fits and the category of the polyethylene: the Gaussian fit was significantly better (lower *R*-factor) for the lightly branched grades (homopolymers and HDPE) but was slightly worse (higher *R*-factor) for the more highly branched grades (LLDPE and VLDPE). For consistency, all structural data presented here for the fibres were taken from the Gaussian fits.

True crystallinity values could not be calculated for the fibre patterns but a related estimate was obtained, referred to here as the crystallinity index, which was internally consistent between the fibre samples. The problem was that in fitting to the fibre diffraction patterns, the fit to the amorphous halo also contained the fit to the incoherent background scatter, and could not be separated from it. Therefore the intensity of the amorphous halo was over-estimated. Accordingly, using the crystallinity estimate method described earlier for the unoriented samples, the fibre crystallinity estimates, termed crystallinity indexes, were considerably under-estimated. In reality, fibres are anticipated to have higher crystallinity values than the equivalent unoriented samples [67,68], and this was indeed seen from the DSC crystallinity values obtained. Nevertheless, the fibre crystallinity index values provided an internally consistent means of evaluating crystallinity variations between the fibre samples, for comparison with the unoriented samples. The limitations of the fibre crystallinity estimates, however, cannot be overstressed.

3. Results and discussion

3.1. TREF: the variation in sample branch distribution

The branching distribution parameters obtained from the TREF analysis, viz. $\bar{N}_w$, $\bar{N}_n$ and $\bar{N}_w/\bar{N}_n$ are shown in Fig. 1.

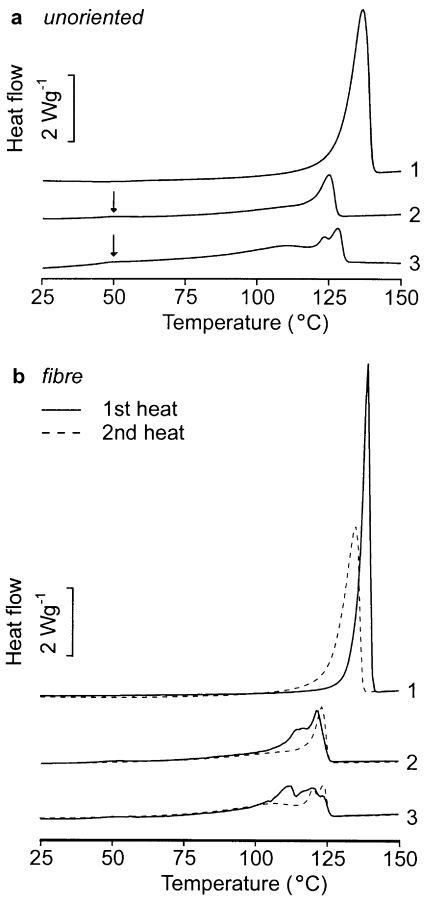

Fig. 2. (a) The three types of DSC trace found in the unoriented polyethylene samples (first heat). (b) The DSC traces from fibres (first and second heats) for the same three grades as shown in (a). Curve type 1: homopolymer and HDPE grades; 2: LDPE and some LLDPE grades; 3: other LLDPE grades and VLDPE. The arrows in (a) mark the approximate position (50°C) of the additional weak endotherm seen in curve types 2 and 3 (unoriented and fibre samples).

The branching distribution analysis method is valid only for cases where the maximum methylene sequence length between branches in a chain is less than the equilibrium crystal thickness under the conditions used [21]. The acceptable range for this [21] is $\bar{N} \leq 250$, satisfied by all the seven LLDPE grades and one VLDPE grade examined here, as confirmed in Fig. 1a. Fig. 1a shows that, as expected, both the number and weight averages of CH_2 units between branch points, $\bar{N}_n$ and $\bar{N}_w$, decreased significantly as the sample branch content increased. Fig. 1b shows the variation in branch distribution parameter $\bar{N}_w/\bar{N}_n$ for the samples. A rise in $\bar{N}_w/\bar{N}_n$ from the lower limit of 1.0 indicates a gradual transition in the distribution of branches from uniform (1.0), through random (in the range 1.1–1.3), to increasing levels of heterogeneity (values higher than 1.3) in the branch placement [69]. Fig. 1b demonstrates a wide variation in the placement of the branches and to a reasonable estimate, three of the LLDPE grades can be described as random and the other four grades and the VLDPE grade as heterogeneous in branch distribution, as labelled in Fig. 1b and Table 1.

Ideally, in order to investigate the effects of branch distribution on the structure of polyethylene, model series are required where samples have fixed branch content and chain length and differ only in how the branches are distributed along the chains. Such model series were not available for this study and there are no reports in the literature of investigations into the structural effects of branch distribution. However, examination of Table 1 shows that the branch contents of the seven LLDPE grades were in the relatively narrow range of 12.4–18 SCB/1000C whilst the $\bar{N}_w/\bar{N}_n$ parameters were in the relatively broad range of 1.36–1.92 indicating near randomness to strong heterogeneity in branch distribution. In the circumstances, it was felt acceptable to treat these seven LLDPE samples as having the same branch content in order to obtain a preliminary study of branch distribution effects via use of the $\bar{N}_w/\bar{N}_n$ parameter. It was necessary in the analyses to assume the seven LLDPE samples differed only in branch distribution: effects of differences in molecular weight, for example, or the type of branch placement heterogeneity, whether intramolecular or intermolecular (as discussed in the Introduction) had to be ignored. We hope that as model polyethylene ranges become available, further, more complete studies of branch distribution effects will be possible.

3.2. DSC

3.2.1. The number of melting peaks

DSC scans of the unoriented samples revealed three types of melting curve, as illustrated in Fig. 2a. A single melting peak existed for the HDPE grades, whether homopolymer or methyl-branched (trace 1 of Fig. 2a). An additional small peak around 50°C appeared for all LDPE, LLDPE and VLDPE grades (trace 2), and two further peaks in the region of the main melting peak (i.e. a total of 3) were seen for four of the LLDPE grades (eth-16, isob-14, hex-12, hex-14a) and the VLDPE grade (eth-31) (trace 3). Branching in the polyethylene samples therefore produced additional broader and smaller endotherms at lower temperatures. This could imply a multi-modal distribution of either crystallite size or crystallite structure. In polyethylene the former explanation is generally accepted, namely that each peak represents a different population of lamellar thickness [45]. From the positions of the highest melting peaks, the lamellar thicknesses were estimated from the Thomson–Gibbs equation to be in the range 60–230 Å. It might be anticipated that the number of melting peaks in the LLDPE grades may be related to the extent of heterogeneity in branch distribution. To test this, the data points in Fig. 1b are identified according to the number of melting peaks: the grades which showed three melting peaks are identified with an asterisk; the other grades showed a single melting peak in the region of 125°C. However, this reveals no relationship between the two characteristics. Instead the two types of melting curves

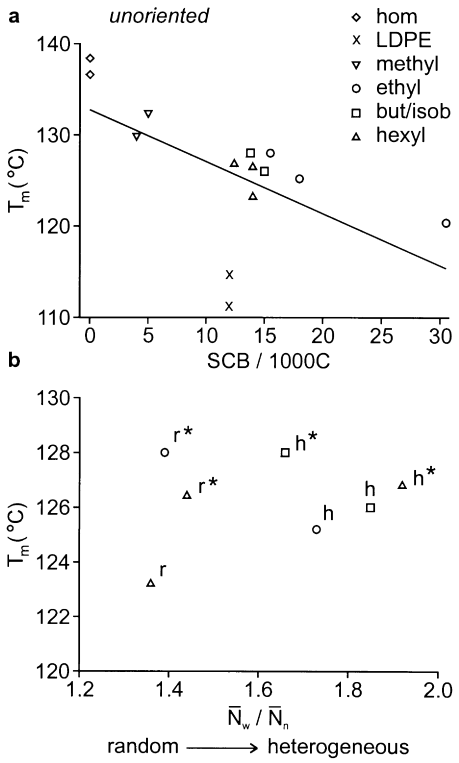

Fig. 3. The melting temperature, T_m, from DSC of the unoriented samples as a function of (a)branch content and (b) branch distribution (the seven LLDPE grades only). The data-points in (b) identified by * indicate grades where the main melting endotherm was divided into three peaks (refer to Figs. 1 and 2). The estimated error bars for T_m were of a similar size to the symbols. The slope of the linear regression fit in (a) was significantly different from zero ($P < 0.05$, *t*-test). The plots show a decrease in T_m with increasing branch content but no evidence of a dependence of T_m on branch distribution is seen. Those samples which showed multiple melting peaks in the main DSC endotherm are seen to have higher T_m than samples which showed a single melting peak.

for the LLDPE samples could possibly be ascribed to differences in polymerisation conditions.

The DSC scans from the oriented samples relative to those from the unoriented samples can be compared in Fig. 2b. This shows that the DSC scan from the fibres on the second heating run correlated closely with that from the equivalent unoriented sample in Fig. 2a. This confirms that, as expected, most of the uniaxial orientation was lost during the first heat into the melt. The range of lamellar thickness in the fibre samples, indicated by the melting peak positions using the Thomson–Gibbs equation, was 60–260 Å. For many samples, particularly those with higher levels of branching, the DSC traces from the fibre samples were not as well defined as from the unoriented samples and this was attributed to progressive relaxation of the unrestrained fibres during heating.

Overall, the DSC traces from the fibres fell into two categories. For both homopolymer and methyl-branched HDPE grades, the first heat melting endotherms were narrower and elevated in temperature relative to the unoriented samples, as shown by curve 1 in Fig. 2b. The higher melting points indicated longer crystal lengths after drawing [70,71] consistent with the presence of strained tie molecules [72]. For the LDPE, LLDPE and VLDPE grades, the first heat melting endotherms were broader, less clearly defined and the melting peak position was often depressed slightly relative to the equivalent unoriented sample; in addition the size of the small endotherm at around 50°C was enhanced. The melting point depression phenomenon persisted for the second heat. The more highly branched grades, which in unoriented form had shown a single melting peak around the melt region, developed an additional peak on the low temperature side of the endotherm (see curve 2 in Fig. 2b), indicating that drawing had caused an additional population of thinner crystallites to develop. Those grades which had shown three peaks in unoriented form did not develop extra peaks upon drawing; the peaks generally remained in the same positions and the lower temperature peaks merely became more intense (see curve 3 in Fig. 2b). The two categories of fibre melting curves, for the HDPE grades and for the more heavily branched grades (LDPE, LLDPE, VLDPE), may be a reflection of the different lamellar deformation mechanisms proposed under cold drawing conditions for these materials [73].

3.2.2. Melting temperature

The dependence of the melting temperature, T_m (and thus also lamellar thickness, from the Thomson–Gibbs equation), on branch content, type and distribution for the unoriented samples are shown in Fig. 3. The plots for oriented samples (not shown) were similar to those for the unoriented samples. Fig. 3a reveals a significant decrease in T_m with increasing branch content ($P < 0.05$, *t*-test on regression slope). Fig. 3a also indicates a possible dependence of T_m on branch type, seen within the LLDPE samples around 15 SCB/1000C. For similar branch contents, longer branches produced a lower T_m. The two LDPE samples show considerably lower T_m than expected from their branch contents, even allowing for a wide margin of error in their estimated branch content. This is probably caused by the long chain branching (heptyl branches and longer) known to be present in LDPE from its polymerisation mechanism.

Fig. 3b shows no evidence for a relationship between T_m and branch distribution. However, for the three LLDPE grades which showed a single melting peak (data points without an asterisk; data points with an asterisk had three melting peaks), where the peak temperature could be measured with greater precision, an indication is seen of a possible increase in T_m with increasing heterogeneity. An effect of branch distribution on T_m has been proposed before as an explanation for the range of T_m values found in polyethylenes with similar branch contents which had been produced by different polymerisation processes [74,75]. The corresponding trend of a tentative increase in lamellar thickness with increasing heterogeneity is plausible because of the longer methylene sequence lengths which exist

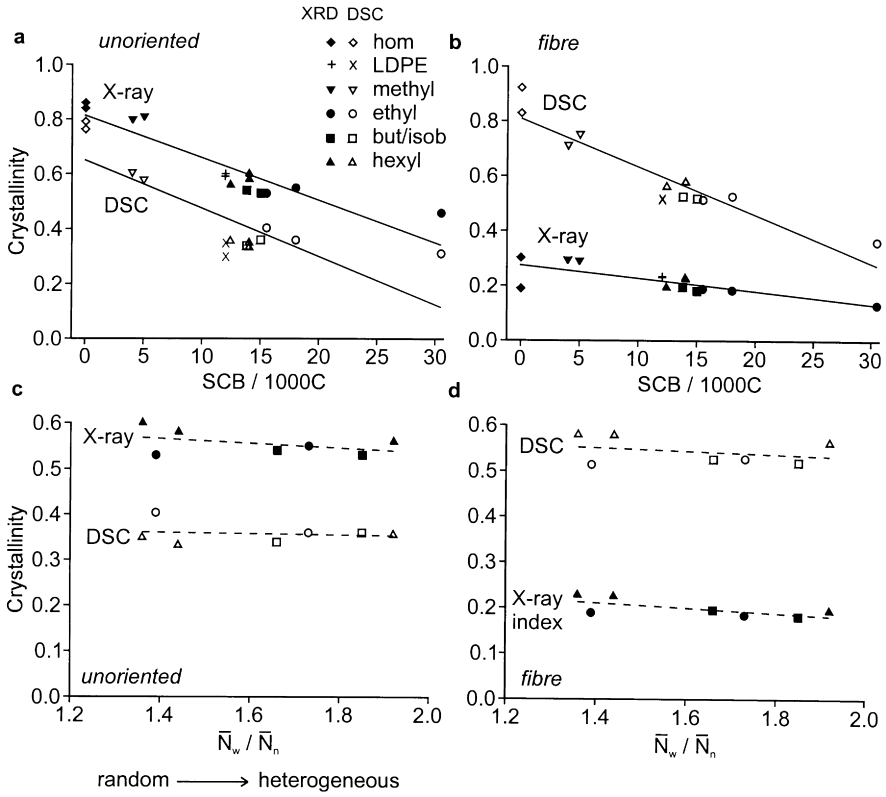

Fig. 4. The crystallinity values from DSC (open symbols) and X-ray diffraction (solid symbols). The values are shown as functions of branch content in (a) & (b), and branch distribution in (c) & (d). Unoriented samples are shown in (a) & (c) and fibre samples in (b) & (d). The linear regression fits are shown by a solid line if the slope was significantly different from zero ($P < 0.05$, *t*-test), dotted otherwise. The label 'X-ray index' for the fibre samples refers to the fact that the X-ray crystallinity values from the fibre samples were not true estimates of crystallinity: they were under-estimates but are internally consistent. The plots show a significant decrease in crystallinity with increasing branch content but no evidence of a dependence on branch distribution is seen.

between some of the branch points in more highly heterogeneous polyethylenes.

3.2.3. Degree of crystallinity

The degree of crystallinity values calculated from the DSC traces for the unoriented samples are shown in Fig. 4, as functions of branch content (Fig. 4a) and branch distribution (Fig. 4c). The equivalent plots for the fibre samples are shown in Fig. 4b and d, respectively. For comparison with the DSC crystallinity estimates, the crystallinity values calculated from the unoriented X-ray diffraction patterns are superimposed in Fig. 4a and c, as are the crystallinity index values from the oriented samples in Fig. 4b and d.

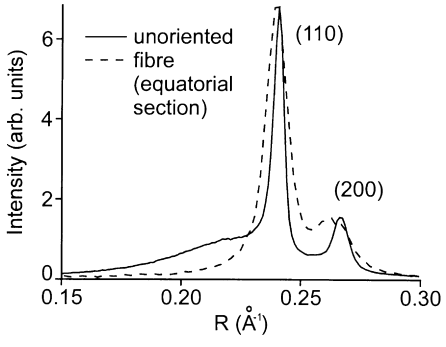

Fig. 5. The (110) and (200) reflection regions from the X-ray diffraction patterns of a LLDPE (eth-16, 16 ethyl SCB/1000C) in unoriented and fibre forms. The fibre data are taken from an equatorial section through the fibre diffraction pattern. The drawing process is seen to broaden and shift the two reflections.

Comparison of the DSC crystallinity values demonstrates that crystallinity was increased by the drawing process, probably from strain-induced crystallisation in the amorphous component [68]. The X-ray crystallinity values do not reproduce this trend because the values calculated from the fibre diffraction patterns were not true estimates of crystallinity. As described earlier, from their method of calculation they were known to be an under-estimate of true crystallinity and were accordingly termed crystallinity index values. However, in comparing the values between branch types, the crystallinity trends from the different techniques are self-consistent.

All crystallinity estimates in Fig. 4 show that crystallinity dropped considerably as the level of branching increased. No clear evidence of a dependence between crystallinity and branch distribution is found in Fig. 4c and d although a dependence has been previously proposed [76]. A possible effect of branch type is seen in Fig. 4c and d: the hexyl branched grades generally show higher crystallinities than the shorter ethyl, butyl and isobutyl branched grades. The

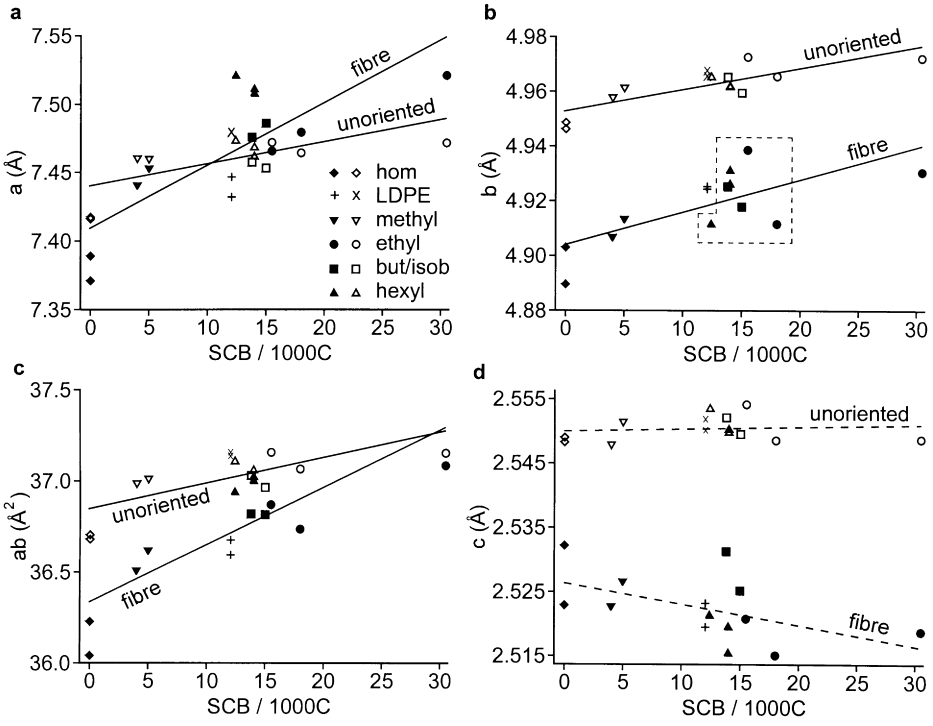

Fig. 6. The unit cell parameters *a*, *b* and *c* and the unit cell basal *ab*, respectively, calculated from the unoriented and fibre X-ray diffraction patterns (using reflections in the range 28–60°2θ i.e. excluding (110) and (200)), as a function of branch content. The error bars were of a similar size to the symbols for the unoriented samples; error bars for the fibres were not available. The linear regression fits are shown by a solid line if the slope was significantly different from zero ($P < 0.05$, *t*-test), dotted otherwise. The plots show a significant increase in *a*, *b* and *ab* with increasing branch content, from both unoriented and fibre samples; a decrease in *c* is indicated from the fibre samples. The boxed area in (b) identifies the seven LLDPE grades which feature in Fig. 7.

disruption of crystallinity in LLDPE samples has been reported to be independent of the branch type [16]. Overall, it is generally reported that crystallinity is sensitive to branch content, independent of branch type and may be affected by branch distribution [20,75].

3.3. X-ray diffraction

The general effects of the drawing process on the X-ray diffraction pattern of polyethylene can be seen in Fig. 5. This compares the region of the (110) and (200) reflections from the unoriented diffraction pattern of one of the LLDPE grades, eth-16, with the corresponding equatorial section through the fibre diffraction pattern. After drawing, the (110) and (200) reflections are broadened, indicating increased strain and/or a reduction in crystallite size, and are also shifted slightly in position from the unoriented sample, indicating a change in unit cell parameters. These two reflections were actually omitted from the fitting procedure because they were believed to be affected by the presence of a partially ordered component (see following paper [25]).

The results of pattern fitting from both unoriented and fibre samples are summarised in Figs. 6 and 7. These figures show for all the grades how the three unit cell parameters *a*, *b* and *c* and the basal area *ab* (refined by pattern fitting using reflections in the range 28–60°2θ) were related to branch content and distribution, respectively, and affected by fibre drawing; the effect of branch type is shown in the figures by different graph symbols. The three effects of branch content, distribution, and type are discussed separately in the following sections.

3.3.1. Effect of branch content

Fig. 6 shows a general increase in the unit cell parameters of both the unoriented and fibre samples with increasing branch content; an exception is the *c* parameter. The values from the fibre samples covered wider ranges than from the unoriented samples and so the fibres were more sensitive for detecting influences of branch content, type and distribution. The increase in the *a* and *b* unit cell parameters with increasing branch content is well known for unoriented polyethylenes [3–15,17] and has also been reported for oriented polyethylene [17]. Regarding the *c* parameter, for the unoriented samples in Fig. 6d, no dependence of *c* on the branch content is seen, although in the fibre samples a possible decrease in *c* was seen in moving from the homopolymer HDPEs towards higher levels of branching. The constancy in the *c* parameter for unoriented samples has been reported before [6], but the decrease in *c* for fibre samples is less well known [17] and is thought to be related to the negative thermal expansion coefficient of the *c*-axis [77]. The effects of branching and temperature on the unit cell parameters of

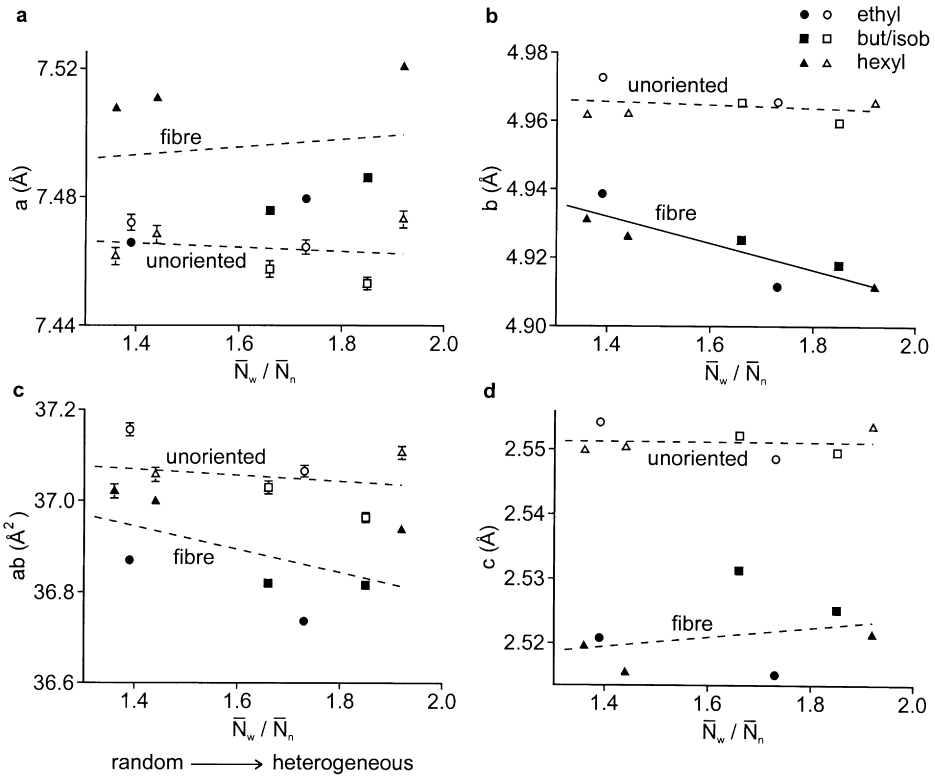

Fig. 7. The unit cell parameters *a*, *b* and *c* and the unit cell basal area *ab*, respectively, calculated from the unoriented and fibre sample X-ray diffraction patterns (using reflections in the range 28–60°2θ i.e. excluding (110) and (200)), as a function of branch distribution. The seven grades featured are LLDPEs with similar branch contents, identified by the boxed area in Fig. 6b. Error bars are shown for the unoriented samples in (a) and (b) whereas in (c) and (d) they were of a similar size to the data point symbols and are therefore not shown. Error bars for the fibre sample data were not available. The linear regression fits are shown by a solid line if the slope was significantly different from zero ($P < 0.05$, *t*-test), dotted otherwise. The fibre samples are seen to have been more sensitive to the influence of branch distribution. The plots show a significant decrease in *b* with increasing heterogeneity in branch placement, for the fibre samples; a similar decrease is indicated by the *ab* unit cell basal area.

polyethylene have been previously recognised to be similar [6,78].

Regarding the effect of drawing on the unit cell parameters, Fig. 6a shows that for the homopolymer, HDPE and LDPE grades, drawing reduced the *a* unit cell parameter whereas for the more highly branched LLDPE and VLDPE grades drawing had the opposite effect. Fig. 6b shows that for all grades, the *b* unit cell parameter values from the fibre samples were considerably lower than from the unoriented samples. The cumulative effect of the changes in *a* and *b* parameters on the unit cell basal area, *ab*, (equal to twice the effective cross sectional area per chain) is illustrated in Fig. 6c. This shows a consistent reduction in basal area with drawing for all grades which was greatest for the grades containing few or no branches i.e. the homopolymer and HDPE grades. The *c* parameter, like the *b* parameter and the product *ab*, showed a reduction for all grades upon drawing. Thus the crystalline density was increased by drawing. The opposite trends of an increase in *a* and *b* cell parameters and a decrease in crystalline density with drawing have been previously reported [17,33] although this may be related to the difference in drawing conditions used.

The increase in *a* and *b* unit cell parameters with branch content has frequently been assumed to indicate incorporation of the branches into the crystalline material (see for example Ref. [6]). An alternative, less common, explanation for these unit cell parameter expansions is stress on the lamellae surfaces caused by branch rejection [17,79]. However, the unit cell parameters have also been shown to vary inversely with the lamellar thickness [31,77]. This effect is not generally recognised and has not been accounted for in such investigations of branching, yet it is widely known that branching reduces the crystallite thickness of polyethylene, as confirmed here by Fig. 3 (from the Thomson–Gibbs equation, the crystallite thickness is inversely related to the melting temperature T_m). The magnitude of the variation in unit cell parameters anticipated from the known reduction in crystallite thickness was estimated here according to the work of Davis et al. [77], as outlined below.

Application of the Thomson–Gibbs equation to the T_m data of Fig. 3 indicates that the lamellar thicknesses of the unoriented samples lay in the approximate range 60–230 Å and a similar range was found for the fibre samples (60–260 Å). From the data of Davis et al. [77], this variation in lamellar thickness of about 200 Å should at room temperature produce a difference in *ab* of 0.3 Å^2. From Fig. 6c, the

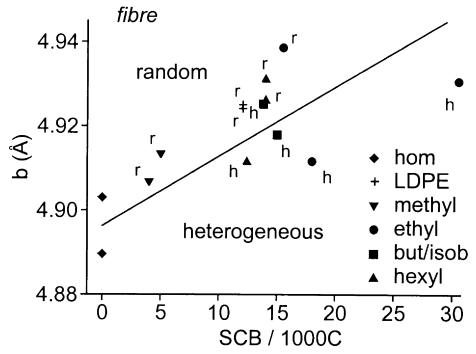

Fig. 8. The *b* unit cell parameter values calculated from the fibre X-ray diffraction patterns as function of branch content. The data-points are labelled according to whether the samples were approximately random (r) or approximately heterogeneous (h) in branch placement. The slope of the linear regression fit was significantly different from zero ($P < 0.05$, *t*-test). Randomly branched samples tend to lie above the regression fit and heterogeneous samples below.

actual variation across the unoriented samples was 0.5 $Å^2$ and across the fibre samples was 1.0 $Å^2$. Thus the expansion in the unit cell basal area *ab* with increasing branch content was not likely to be attributable solely to the reduction in lamellar thickness. As described in the final paper in this sequence [26], changes were found in some of the reflection intensity ratios measured in the X-ray diffraction patterns,

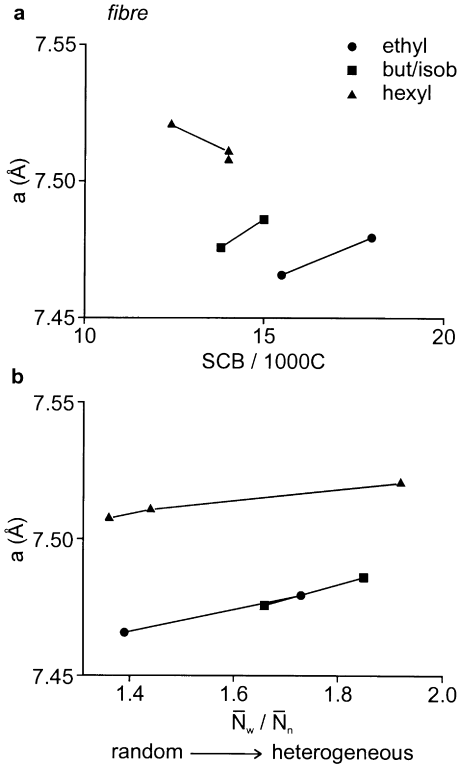

Fig. 9. The effect of branch type in the *a* unit cell parameter of the LLDPE fibre samples as a function of (a) branch content and (b) branch distribution. It appears that for similar branch contents, hexyl branches cause more expansion than butyl or isobutyl branches and least expansion is seen by ethyl branches.

and were shown from molecular modelling to be consistent with the incorporation of some branches into the crystalline material. The additional unit cell expansion seen is therefore probably explained by the inclusion of branches rather than by the branches affecting the structure in some other way.

3.3.2. Effect of branch distribution

Fig. 7 examines the relationship between the unit cell parameters and the distribution of branches, for the seven LLDPE grades with similar branch contents shown within the boxed area in Fig. 6b. The scatter in the data points is severe and the only change, which reached statistical significance, was a decrease in the *b* unit cell parameter from the fibre samples with increasing heterogeneity in branch placement. A similar decrease is indicated by the *ab* basal area values in both the unoriented and fibre samples. The possible decrease in some of the unit cell parameters with higher levels of heterogeneity is plausible because heterogeneity is consistent with a broader distribution of methylene sequence lengths and thus the presence of some longer methylene sequence lengths, with the potential for thicker crystallites. The presence of thicker lamellae with more heterogeneous branching distributions was independently indicated by the DSC melting temperature data in Fig. 3b.

To investigate this tentative effect of heterogeneity further, Fig. 8 replots the *b* unit cell parameter values as a function of branch content from Fig. 6b for the fibre samples (the only unit cell parameter versus $\bar{N}_w/\bar{N}_n$ trend in Fig. 7 which reached significance). The samples are classified as being random 'r' or heterogeneous 'h' in branch distribution according to Table 1; the line shows the regression calculated across all points. The scatter in the cell parameter values in Fig. 8 is clearly seen to be explained by the variation in the distribution of branches: randomly distributed branches enhance the extent of cell parameter expansion over heterogeneously distributed branches for similar branch contents.

Returning to Fig. 7, most of the unit cell parameters, particularly those from the unoriented samples, indicate no change with heterogeneity although this may be because of the few data points. A statistically significant decrease is seen in the *b* unit cell parameter from the fibre samples with increasing heterogeneity and a decrease is possibly indicated in the *ab* basal area too. When the branch type of the samples is taken into account, the *a* unit cell parameter from the fibre samples indicates a possible increase with increasing heterogeneity. This is shown more clearly in Fig. 9.

3.3.3. Effect of branch type

Fig. 9a shows the *a* unit cell parameter from the seven LLDPE fibre samples as a function of branch content. It demonstrates that for the similar levels of branching present in these samples (15 ± 3 SCB/1000C), hexyl branches produced a larger expansion than butyl or isobutyl branches which in turn produced a larger expansion than ethyl

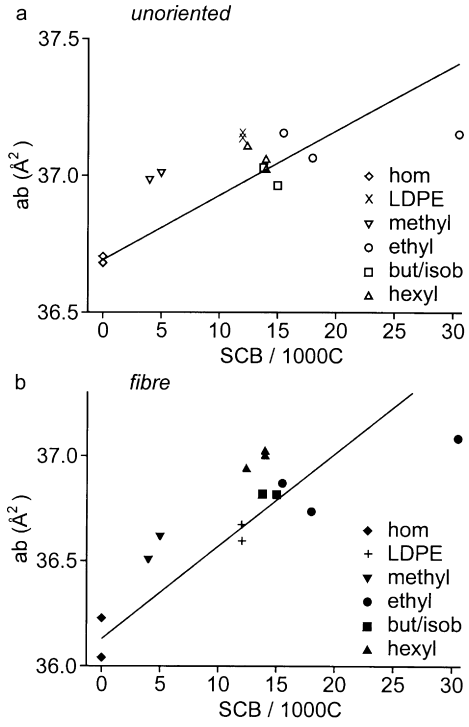

Fig. 10. The *ab* unit cell basal area as a function of branch content for (a) unoriented and (b) fibre samples. The slopes of the linear regression fits were both significantly different from zero ($P < 0.05$, *t*-test). The plots indicate that for a given branch content, methyl branches cause higher expansion than longer branches.

branches. In Fig. 9b, all three branch types appear to indicate an increase in expansion with increasing heterogeneity, for similar branch contents but this cannot reach statistical significance with so few data points for each branch type. Furthermore, even the overall trend in the *a* unit cell parameter of the fibre samples as a function of $\bar{N}_w/\bar{N}_n$ failed to reach significance (see Fig. 7a).

This apparent dependence on branch type of unit cell expansion in polyethylene for ethyl and longer branches has not been reported before. Instead it is widely reported that for any specific branch content, methyl branches cause more expansion than longer branches, with the longer branches all causing similar amounts of expansion. Fig. 10 replots the expansions in the *ab* unit cell basal area as a function of branch content as in Fig. 6c but in Fig. 10 the *y*-intercept of the linear regression lines are forced through the midpoint of the homopolymer values, unlike the free fits in Fig. 6c. This has been done because the homopolymer grades were considered relatively reliable: there was little potential error in their branch content values (since these were very close to zero). Unfortunately, higher methyl branch content polyethylenes were not available for examination, nor were lower branch concentration polyethylenes containing longer branches. The methyl branched samples do, however, indicate a higher than expected expansion. Within the longer branches, the hexyl branched fibre samples show unusually high expansion but the effect is less clear in the unoriented samples. Remembering the relatively weak effect of branch placement on unit cell parameter expansion seen in Figs. 7 and 8, it is unlikely that the larger expansion in the methyl branched samples could have been caused solely by a higher degree of randomness in branch distribution compared with the LLDPE and LDPE grades containing longer branches. The LDPE grades (containing mainly ethyl and butyl branches) are known to be the most ideally random category examined here and even allowing for inaccuracies in their branch content estimate, the methyl-branched HDPE samples showed larger expansions than expected on the basis of their branch contents.

4. Conclusions

The effects of branch content, type and distribution on the crystal structure of polyethylene have been examined using X-ray diffraction and differential scanning calorimetry (DSC). A broad range of polyethylenes was used, in both unoriented and uniaxially drawn forms: the drawing was found generally to cause a decrease in all three unit cell parameters. The effect of branch distribution is seldom considered but here a quantitative analysis was made: a parameter describing heterogeneity in branch distribution was derived from analytical TREF data using the method of Bonner et al. [21].

From DSC of the polyethylenes, an increase in melting temperature was indicated for samples with higher levels of heterogeneity in branch distribution. No relationship was found, however, between the number of peaks in the melting endotherm of a sample and its extent of heterogeneity. Crystallinity values estimated from both the X-ray diffraction and DSC data were found to be determined primarily by the branch content, showing a reduction for higher branch contents. No dependence on branch distribution was found. An effect of branch type was indicated by the LLDPE samples: for similar branch contents, grades containing longer (hexyl) branches showed higher crystallinities than grades containing shorter (butyl, isobutyl or ethyl) branches.

Regarding the crystal structure, branch content was found to be the most influential parameter, with significant increases in the *a* and *b* unit cell parameters and the *ab* unit cell basal area with increasing branch content. From the fibre samples, a decrease was seen in the *c* unit cell parameter. Considerable scatter was evident in all the data-points. The increases in the *a*, *b* and *ab* parameters could not be accounted for fully by the reduction in crystallite thickness determined from the DSC data but could be accounted for by the crystalline incorporation of some branches (the focus of one of the following papers in this sequence [26]). The scatter in data-points was found to be explained by the variations in branch distribution between the samples: more unit cell parameter expansion was seen from a random distribution of branches than from a

heterogeneous distribution. Regarding branch type, most unit cell parameter expansion was seen by methyl branches, as has been reported previously. More unusually, a difference between ethyl and longer branches was revealed by the fibre samples, where for the *a* unit cell parameter most expansion was seen by hexyl branches and least by ethyl branches.

Finally, X-ray diffraction patterns are routinely corrected for Lorentz and polarisation effects but in polymers the addition errors incurred by transparency of the sample to X-rays are seldom considered. Following the method first proposed by Langford and Wilson [54], it has been found here that, using data collection conditions not atypical of those generally used for polymers, correcting for sample transparency in polymer X-ray diffraction work is comparable in importance to the correction for polarisation and should therefore be routinely applied.

Acknowledgements

The authors wish to thank BP Chemicals for the TREF analysis, Mary Vickers for valuable discussions, Simon Hanna for advice concerning the fibre X-ray diffractometer, Chris Frye for supplying the materials and Brain Seymour, John Carter, Keith Page and Joe Ellis for technical support. The fibre diffraction patterns were analysed using the CCP13 suite of programs (CCLRC Daresbury Laboratory) and advice from Richard Denny and Gabriel Welsh is gratefully acknowledged. The work was supported by an EPSRC Research Studentship and CASE Award from BP Chemicals (AMEB).

Appendix A

The usual correction factors applied to X-ray diffraction data from polymers are Lorentz and polarisation factors. However, the low-mass absorption coefficient of polymers causes diffraction to be recorded from throughout the thickness of the sample, incurring additional errors. Assuming perfect surface alignment, the diffraction data collected from polymers represent undistorted data from the sample surface superimposed on distorted data from the internal sample layers, the diffraction from each layer being weighted in intensity because of attenuation by absorption through the sample. A comprehensive analysis and correction procedure for this has been presented by Langford and Wilson [54]. The sample thicknesses examined here were sufficient to suspect data distortion by transparency effects and so this correction procedure was applied. For the X-ray diffraction conditions used here, the effective depth of penetration was less than the sample thickness and so the relevant transparency correction factor was [54]

$$F(\rho,\sigma) = 1 - \rho^{-1}\sinh\rho\exp(-\sigma) \quad \text{(A1)}$$

where $\rho = \alpha\mu R \operatorname{cosec} 2\theta$ and $\sigma = \omega\mu R \operatorname{cosec} 2\theta$; α was the divergence slit (0.3°), ω the receiving slit (0.15°), μ the linear absorption coefficient (in the range 3.845 g cm^{-4} [HDPE] to 3.645 g cm^{-4} [VLDPE]), R the goniometer radius (200.5 mm) and θ the Bragg angle.

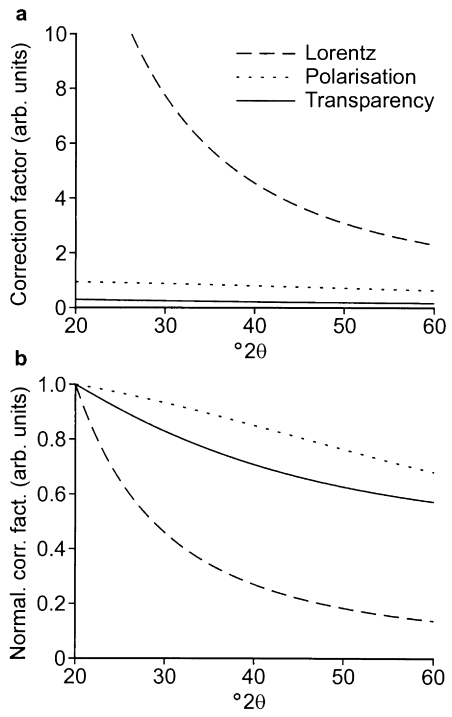

Fig. A1. Comparison of the Lorentz, polarisation and transparency correction factors for the X-ray reflection mode conditions used in this study. (a) shows the factors on an absolute scale. In (b) the factors have been normalised with respect to their values at 20°2θ. The Lorentz factor is given by $1/(\sin 2\theta \sin\theta)$. The polarisation factor is given by $(1 + \cos^2 2\theta_m \cos^2 2\theta)/(1 + \cos^2 2\theta_m)$ where θ_m is the Bragg angle for the monochromator (8.7° for graphite). The transparency factor is $F(\rho,\sigma)$ (shown here for the HPDE samples), calculated from the method of Langford and Wilson [54].

The magnitude of the correction was then compared with that of the Lorentz and polarisation factors [66] to deduce the relative importance of the correction. The three correction factors are shown in Fig. A1a and normalised in Fig. A1b where the relationship between the correction factors and the observed and corrected intensities, I_o and I_c, respectively, is

$$I_o = LPF(\rho,\sigma)I_c \quad \text{(A2)}$$

where L is the Lorentz factor, P the polarisation factor and $F(\rho,\sigma)$ the transparency factor. Fig. A1b reveals that for the samples and conditions used here, which were not atypical of the X-ray diffraction conditions generally used for polymers, the Lorentz correction was the most important to apply and the correction for transparency was comparable in importance to the correction for beam polarisation. Both Lorentz and polarisation factors are considered essential and are routinely applied for accurate X-ray diffraction work. Correction for sample transparency in polymers is in

many instances therefore also likely to be important, although it is seldom considered.

References

[1] Soares JBP, Hamielec AE. Polymer 1995;36:2257–63.
[2] Kakugo M, Naito Y, Mizunuma K, Miyatake T. Makromol Chem 1989;190:849–64.
[3] Walter ER, Reding FP. J Polym Sci 1956;21:561–2.
[4] Eichhorn RM. J Polym Sci 1958;31:197–8.
[5] Cole EA, Holmes DR. J Polym Sci 1960;46:245–56.
[6] Swan PR. J Polym Sci 1962;56:409–16.
[7] Wunderlich B, Poland D. J Polym Sci (A1) 1963;1:357–72.
[8] Richardson MJ, Flory PJ, Jackson JB. Polymer 1963;4:221–36.
[9] Bodily D, Wunderlich B. J Polym Sci (A2) 1966;4:25–40.
[10] Baker CH, Mandelkern L. Polymer 1966;7:71–83.
[11] Holdsworth PJ, Keller A. Polym Lett 1967;5:605–12.
[12] Kavesh S, Schultz JM. J Polym Sci (A2) 1970;8:243–76.
[13] Shirayama K, Kita S-I, Watabe H. Makromol Chem 1972;151:97–120.
[14] Vonk CG. J Polym Sci (C) 1972;38:429–35.
[15] Preedy JE. Br Polym J 1973;5:13–9.
[16] Burfield DR, Kashiwa N. Makromol Chem 1985;186:2657–62.
[17] Howard PR, Crist B. J Polym Sci (Phys) 1989;27:2269–82.
[18] Gerum W, Hohne GWH, Wilke W, Arnold M, Wegner T. Macromol Chem Phys 1996;197:1691–712.
[19] Mirabella FM, Ford EA. J Polym Sci (Phys) 1987;25:777–90.
[20] Alamo RG, Mandelkern L. Therm Acta 1994;238:155–201.
[21] Bonner JG, Frye CJ, Capaccio G. Polymer 1993;34:3532–4.
[22] Glockner G. J Appl Polym Sci, Appl Polym Symp 1990;45:1–24.
[23] Wild L. Adv Polym Sci 1991;98:1–47.
[24] Soares JBP, Hamielec AE. Polymer 1995;36:1639–54.
[25] Baker AME, Windle AH. Polymer 2000;42:667–80.
[26] Baker AME, Windle AH. Polymer 2000;42:681–98.
[27] Hansen EW, Blom R, Bade OM. Polymer 1997;38:4295–304.
[28] Bovey FA, Schilling FC, McCrackin FL, Wagner HL. Macromolecules 1976;9:76–80.
[29] Dorman DE, Otocka EP, Bovey FA. Macromolecules 1972;5:574–7.
[30] Cudby MEA, Bunn A. Polymer 1976;17:345–7.
[31] Davis GT, Eby RK, Martin GM. J Appl Phys 1968;39:4973.
[32] Fischer EW, Goddar H, Schmidt GF. J Polym Sci (A2) 1969;7:37–45.
[33] Glenz W, Morosoff N, Peterlin A. Polym Lett 1971;9:211–7.
[34] Perkins WG, Porter RS. J Mater Sci 1977;12:2355–88.
[35] Ward IM. In: Ward M, editor. Developments in oriented polymers, vol. 1. London: Applied Science, 1982.
[36] Hall IM, Toy M. In: Hall IM, editor. Structure of crystalline polymers, London: Elsevier, 1984. p. 181–228.
[37] Dupuis J, Legrand P, Seguelat R, Rietsch F. Polymer 1988;29:626–33.
[38] Lin L, Argon AS. J Mater Sci 1994;29:294.
[39] Bartczak Z, Galeski A, Argon AS, Cohen RE. Polymer 1996;37:2113–23.
[40] Meinel G, Peterlin A. J Polym Sci 1971;9:67.
[41] Wunderlich B. Macromolecular physics. Crystal melting, vol. 3. New York: Academic Press, 1980.
[42] Mathot VBF, Pijpers MFJ. J Appl Polym Sci 1990;39:979–94.
[43] Brandrup J, Immergut EH. Polymer handbook. New York: Wiley, 1989.
[44] Richardson. In: Allen G, Bevington JC, Booth C, Price C, editors. Comprehensive Polymer Science, vol. 1. New York: Pergamon, 1989. p. 867–901.
[45] Wlochowicz A, Eder M. Polymer 1984;25:1268–70.
[46] Keller A, Sawada S. Makromol Chem 1964;74:190.
[47] Keller A, Machin MJ. J Macromol Sci (Phys) 1967;B1:41.
[48] Hill MJ, Keller A. J Macromol Sci (Phys) 1969;B3:153.
[49] Ruland W. Acta Cryst 1961;14:1180–5.
[50] Vonk CG. J Appl Cryst 1973;6:148–52.
[51] Balta-Calleja FJ, Vonk CG. X-ray scattering of synthetic polymers. Amsterdam: Elsevier, 1989 (p. 175–204).
[52] Ryan AJ, Bras W, Mant GR, Derbyshire GE. Polymer 1994;35:4537–44.
[53] Riello P, Fagherazzi G, Canton P, Clemente D, Signoretto M. J Appl Cryst 1995;28:121–6.
[54] Langford JI, Wilson AJC. J Sci Instrum 1962;39:581–5.
[55] Wiles DB, Young RA. J Appl Cryst 1981;14:149–51.
[56] Rietveld HM. J Appl Cryst 1969;2:65–71.
[57] Young RA. In: Young RA, editor. The Rietveld method, Oxford: Oxford University Press, 1993. p. 1–38.
[58] Vickers ME. In: Richards RW, editor. Scattering methods in polymer science, London: Ellis Horwood, 1995. p. 103–52.
[59] Cagliotti G, Paoletti A, Ricci FP. Nucl Instrum 1958;3:223–8.
[60] Bunn CW. Trans Faraday Soc 1939;35:482–91.
[61] Mitchell GR, Lovell R, Windle AH. Polymer 1982;23:1273–85.
[62] Dollase WA. J Appl Cryst 1986;19:267–72.
[63] Hanna S, Windle AH. J Appl Cryst 1995;28:673–89.
[64] Hanna S, Baker AME, Windle AH. Polymer 1998;39:2409–14.
[65] de Wolff PM. J Polym Sci 1962;60:534–6.
[66] Alexander LE. X-ray diffraction methods in polymer science. New York: Wiley, 1969.
[67] Zevin L, Messalem R. Polymer 1982;23:601–4.
[68] Seguela R, Rietsch F. Polymer 1986;27:532–6.
[69] Frye CJ. BP Chemicals, Lavera, France, personal communication, March 1996.
[70] Clements J, Jakeways R, Ward IM. Polymer 1978;19:639–44.
[71] Frye CJ, Ward IM, Dobb MG, Johnson DJ. Polymer 1979;20:1310–2.
[72] Butler MF, Donald AM, Ryan AJ. Polymer 1997;38:5521–38.
[73] Butler MF, Donald AM, Bras W, Mant GR, Derbyshire GE, Ryan AJ. Macromolecules 1995;28:6383–93.
[74] Clas S-D, McFaddin DC, Russell KE, Scammell-Bullock MV. J Polym Sci (Chem) 1987;25:3105–15.
[75] Alamo RG, Mandelkern L. Macromolecules 1989;22:1273–7.
[76] Cozewith C, ver Strate G. Macromolecules 1971;4:482–9.
[77] Davis GT, Eby RK, Colson JP. J Appl Phys 1970;41:4316–26.
[78] Swan PR. J Polym Sci 1962;56:403–7.
[79] Bunn CW. In: Renfrew A, Morgan P, editors. Polythene: the technology and uses of ethylene polymers, London: Iliffe & Sons, 1960. p. 87–130.